NASA TECHNICAL NOTE

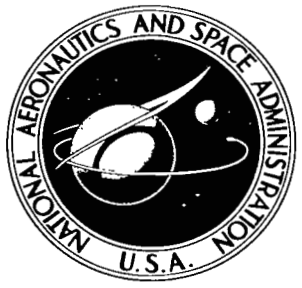

MEASURED AND COMPUTED STATIC AERODYNAMIC CHARACTERISTICS OF ABLATING CONICAL TEFLON MODELS AT MACH NUMBER 14

by Leland H. Jorgensen and Jack R. Hagen

Ames Research Center
Moffett Field, Calif.

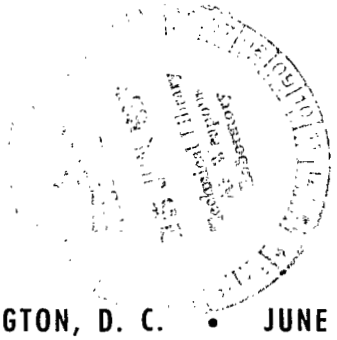

NATIONAL AERONAUTICS AND SPACE ADMINISTRATION • WASHINGTON, D. C. • JUNE 1967

NASA TN D-4022

MEASURED AND COMPUTED STATIC AERODYNAMIC CHARACTERISTICS OF ABLATING CONICAL TEFLON MODELS AT MACH NUMBER 14

By Leland H. Jorgensen and Jack R. Hagen

Ames Research Center
Moffett Field, Calif.

NATIONAL AERONAUTICS AND SPACE ADMINISTRATION

For sale by the Clearinghouse for Federal Scientific and Technical Information
Springfield, Virginia 22151 – CFSTI price $3.00

MEASURED AND COMPUTED STATIC AERODYNAMIC CHARACTERISTICS OF ABLATING CONICAL TEFLON MODELS AT MACH NUMBER 14

By Leland H. Jorgensen and Jack R. Hagen

Ames Research Center

SUMMARY

Axial-force, normal-force, and pitching-moment coefficients were measured for ablating Teflon and nonablating metallic pointed 30° half-angle cones, blunted 10° half-angle cones, and blunted 60° half-angle cones with boattail aftersections. For moderate mass-loss rates up to about 4 percent of the free-stream mass intercepted by the model and with laminar flow, there were no appreciable effects of ablation on the forces and moments. The axial-force coefficients for the 30° half-angle cones were affected the greatest, but they decreased only about 5 percent with ablation throughout the angle-of-attack range studied (0°-20°).

The forces and moments for the pointed 30° half-angle cones were adequately predicted with Newtonian theory. However, for the blunted 10° half-angle cones the predicted normal forces were too small; for the blunt 60° half-angle conical models, the predicted axial forces were too large and the centers of pressure more rearward (by about 0.15 diam) than measured.

A method for estimating recession and mass loss with time is assessed for the present test conditions. Computed curves agree reasonably well with experimental measurements from ablation tests of pointed 10° half-angle cones, 40-percent blunt 10° half-angle cones, and pointed 30° half-angle cones.

INTRODUCTION

In recent years there has been some interest in possible effects of ablation gases on the aerodynamic forces and moments of entry vehicles. Most effort to date has been directed toward simulation of ablation effects for slender cones in hypersonic ballistic reentry flight (e.g., refs. 1-7). In some of the first simulation tests (refs. 1, 2) gas was ejected through holes near the tips of cones mounted in a hypersonic wind-tunnel stream. These early "blowing" tests showed that the initial slopes of static-stability and normal-force curves could be decreased markedly even with low to moderate ejection rates (rates up to only 2 or 3 percent of the free-stream mass intercepted by the cone base). More recent tests of slender cones coated with "mothball-type" material have indicated that actual subliming ablation might produce a loss in static stability but probably little change in normal force

(ref. 7). Tests have indicated also that dynamic stability increases when a slender cone is coated with an ablative material either entirely or only ahead of the center of gravity (refs. 3, 5, and 7). If the material is applied only rearward of the center of gravity, it appears that the cone can become dynamically unstable (ref. 3).

The present investigation was made to measure possible effects of ablation gases on the static forces and pitching moments of three "not so slender" conical configurations. Models of the following shapes were tested: a 40-percent blunt 10° half-angle cone, a pointed 30° half-angle cone, and a slightly blunt 60° half-angle cone with a boattail aftersection. Both metallic nonablating and Teflon ablating models were tested in an arc-heated air tunnel at Mach number 14. Measurements of recession distance, nose radius, and mass loss with time were made for the Teflon models. In this report computed ablation characteristics are compared with those measured from the ablation tests. Then the force and moment results for the ablating and nonablating models are compared.

NOMENCLATURE

A reference area, $\frac{\pi}{4} d^2$

C_A axial-force coefficient, $\frac{\text{axial force}}{q_\infty A}$

C_{m_B} pitching-moment coefficients about balance reference center, $\frac{\text{pitching moment}}{q_\infty A d}$

C_N normal-force coefficient, $\frac{\text{normal force}}{q_\infty A}$

$C_{p_{st}}$ stagnation-pressure coefficient, $\frac{p_{st} - p_\infty}{q_\infty}$

d reference diameter

h enthalpy

h_{eff} effective heat of ablation

k $\frac{\dot{q}_c (h_{eff})_{st}}{\dot{q}_{st} (h_{eff})_c}$, assumed constant

l length of sharp cone

l_a model length after ablation

m	weight or mass loss
$\dot{m}$	$\frac{dm}{dt}$
M	Mach number
p	pressure
q	dynamic pressure, $\frac{1}{2}\rho u^2$
$\dot{q}$	heat-transfer rate
r	nose radius
r_b	base radius
r_o	nose radius without mass loss from side of cone
Re	Reynolds number, $\frac{u_\infty \rho_\infty d}{\mu_\infty}$
t	time
u	speed
V	volume
x	axial distance from cone vertex
x_{cp}	axial distance from model base to center of pressure
α	angle of attack
θ	cone half-angle
μ	coefficient of viscosity
ρ	density

Subscripts

c	cone
cw	cold wall
f	final
hw	hot wall
i	initial

m	material
st	stagnation
t	total
∞	free stream

Conversion From Units in This Report to "SI Units"
(International System of Units, NASA TT F-200)

Physical quantity	To convert from	Multiply by	To obtain
Enthalpy	Btu/lb	2.324×10^3	J/kg
Heating-rate parameter	Btu-ft$^{1/2}$/ft^2-sec	6.266	W-cm$^{1/2}$/cm^2
Length	in.	2.540	cm
Material density	lb/ft^3	16.018	kg/m^3
Pressure	atm	1	atm
Weight loss	lb	0.4536	kg

EXPERIMENTAL APPARATUS, TESTS, AND DATA REDUCTION

Test Facility

All tests were conducted in the Ames arc-heated aerodynamic wind tunnel. The tunnel air was heated with a commercially available Linde N-4000 arc heater, which is essentially a scaled-up version of the Linde 124 heater described in reference 8. A contoured throat section connected the arc-heater unit to a conical nozzle of 8° half-angle and 24-inch exit diameter. For the present investigation a 0.4-inch-diameter throat section was used to obtain a test section Mach number of 14. Heated air from the arc unit was expanded through the nozzle, discharged as a free jet for about 24 inches through the test chamber, and then entrained by a diffuser connected to a five-stage steam ejector system. (Photographs and more details of the facility are given in reference 9.)

Models

Models for preliminary ablation tests were of Teflon and included the following shapes: a 10° half-angle cone (fig. 1(a)), a 40-percent blunt 10° half-angle cone (fig. 1(b)), a 30° half-angle cone (fig. 1(c)), and a blunt 60° half-angle cone with a boattail aftersection (fig. 1(d)). To determine

recession distance, nose radius, and mass loss with time, about six Teflon models of each shape were ablated before the force models were tested. Teflon was used as the ablating material because it sublimes with no melt; all mass loss could thus be considered to leave the body in gaseous form.

The models for the force tests (fig. 2) were the same size as those for the preliminary ablation tests, but they had metallic (nonablating) nose pieces as well as Teflon. Because the mass-loss parameter for the initially pointed 10° half-angle Teflon cone was extremely small ($\dot{m}/\rho_{\infty}u_{\infty}A \approx 0.002$) and the estimated forces and moments were too low for good accuracy with the available balance, no force models of this shape were constructed.

All models were sting-supported from the rear. The force models were mounted on an internal strain-gage balance, 0.75 inch diameter by 2.5 inches long (indicated in fig. 2(a)). The balance, attached to a support connected to the tunnel angle-of-attack mechanism, was designed to measure axial forces up to 10 pounds and normal forces up to 5 pounds.

Test Conditions

The average flow conditions and range of scatter for all test runs are:

M_{∞}	14.0 ±0.1	p_{st}	$(3.45 \pm 0.12)\times10^{-2}$ atm
Re	$(5.8 \pm 0.5)\times10^{3}$/in.	p_t	68.0 ±0.2 atm
h_t	2200 ±300 Btu/lb	$\dot{q}_{st}\sqrt{r}$	17.6 ±1.5 $\frac{\text{Btu-ft}^{1/2}}{\text{ft}^2\text{-sec}}$
q_{∞}	$(1.87 \pm 0.05)\times10^{-2}$ atm		

To determine the Mach number M_{∞}, Reynolds number Re, total enthalpy h_t, and dynamic pressure q_{∞} in the test stream, measurements were made of stagnation (pitot) pressure p_{st}, total (reservoir) pressure p_t, and stagnation heating-rate parameter $\dot{q}_{st}\sqrt{r}$. Then the desired flow parameters were obtained from charts computed from the nonequilibrium nozzle-flow program of reference 10. This program indicated that the nozzle flow in the test region was closer to the frozen state than to the equilibrium state, the frozen Mach number being about 14.5 compared to the equilibrium value of 12.9. The Reynolds number was low (primarily because of the low free-stream density) so the boundary-layer flow over the models was believed to be laminar. A stream survey in the test region showed at least an 8-inch-diameter core of near constant stream properties over the length of the longest model.

The stagnation heating-rate parameter $\dot{q}_{st}\sqrt{r}$ was measured with a hemispherical-nosed calorimeter similar to the one described in reference 9. Total enthalpy h_t was then computed by the Fay and Riddell heating-rate method (ref. 11) as employed in references 9 and 12. The total enthalpy was also determined by the "sonic-flow" method (e.g., refs. 12-14). Values obtained by these two methods generally agreed to within 10 percent for all runs.

Tests

Ablation tests of the Teflon models (fig. 1) were made prior to the force tests. For these ablation tests the models were mounted on a "dummy" balance, and temperatures in the balance region were measured. Over the dummy balance the temperature rise was generally small (usually less than about 35° F) for run times of 30 seconds, the time selected for later tests with the force balance. The model recession distances, nose radii, and mass losses were also measured for run times up to about 100 seconds. To prevent ablation of the models before tunnel running conditions were established, a removable conical shield was placed in front of each model at the start of each run. After the flow was established, a pitot tube and a calorimeter were inserted just ahead of the shield for about 5 seconds to obtain the stream conditions. A few seconds after the pitot tube and calorimeter were removed, the shield was removed, and the ablation (or sublimation) time for the unshielded model was recorded.

After these preliminary ablation tests, force tests of both ablating (Teflon) and nonablating models (fig. 2) were made. Balance measurements of normal force, axial force, and pitching moment with time were recorded for times up to 30 seconds. The conical shield, pitot tube, and hemispherical calorimeter were also used at the start of each run. Models were tested at angles of attack from 0° to about 18° with a separate run for each angle of attack. The mass loss and recession distance for each Teflon model were measured after each run.

For the blunt 60° conical model with the boattail aftersection, an indication of the position of flow separation from the aftersection was determined by the oil-film technique. After the desired stream flow was established in the test section, a light machine oil containing red coloring was pumped from outside the test chamber through a small tube leading to the removable model shield and then out through a spray jet onto the model. After the shield with the jet was removed from the stream, the resulting oil-flow pattern on the model was filmed with a 16-mm movie camera.

Data Reduction

Measurements of normal force, axial force, and pitching moment have been reduced to coefficient form, with the pitching-moment coefficients referred to the balance reference centers which are shown in figure 2. For each run the dynamic pressure, q_∞, used to reduce the data was determined from

$$q_\infty = \frac{p_{st} - p_\infty}{C_{p_{st}}}$$

$$= \frac{p_{st}}{1.85} \qquad (p_{st} \gg p_\infty)$$

The value for $C_{p_{st}}$ was determined from the nonequilibrium nozzle-flow program of reference 10 and was constant throughout the test. Stagnation pressure p_{st} was measured with a pitot tube inserted in the stream just ahead of the model nose at the start of each run. It was also checked with a probe mounted about 3.5 inches radially from the nose. From previous stream surveys it was found that values of p_{st} at these positions agree closely with those at the model nose position. The corresponding values of q_∞ for equilibrium and for frozen flows are

$$q_\infty = \frac{p_{st}}{1.91} \text{ (Equilibrium flow)}$$

$$q_\infty = \frac{p_{st}}{1.83} \text{ (Frozen flow)}$$

These values show that the uncertainty in q_∞ because of uncertainty in flow state was at most only 3 percent. It is believed that any overall inaccuracy in the force and moment coefficients is not much greater than this uncertainty.

RESULTS AND DISCUSSION

In this section, ablation results of recession distance and mass loss with time are presented, and a method for predicting these results is assessed. Then force and moment data for the ablating and nonablating models are presented, and theory for the nonablating shapes is compared with experiment.

Recession Distance and Mass Loss

Experimental results.- For the Teflon ablation models at $\alpha = 0^\circ$, values of recession distance and mass loss increased with time at a nonlinear rate, as shown in figure 3. As expected, the sharp 10° half-angle cone exhibited a much greater recession rate than the 30° half-angle cone and the blunted shapes. However, the mass-loss rate was much lower than for the other shapes since all the ablation from the slender cone occurred at the front where the mass was obviously small. Contours before and after ablation are shown in figure 4. Whereas both the initially sharp and initially blunt 10° half-angle cones ablated only from the front, the 30° and 60° half-angle cones ablated appreciable mass also from the sides. Teflon models expanded slightly upon cooling after each run. Note, for example, the slight contour differences in figures 4(a) and 4(d) where the Teflon pieces connect the steel and copper pieces.

Although the mass loss with time was nonlinear for times up to about 100 seconds (fig. 3), a linear variation could be assumed for times up to about 30 seconds with little error. For times of about 30 seconds, it was also found that the mass loss, as well as the recession distance, was essentially

unchanged with change in angle of attack (see fig. 5). However, with the models at angle of attack, slightly more mass was ablated from the windward side and slightly less from the leeward side than at zero angle of attack. (Note, for example, the contours in figure 6 for $\alpha = 0^\circ$ and $\alpha \approx 15^\circ$.) For a linear variation of total mass loss with time for $t = 30$ seconds, the mass-loss or mass-rate parameter $\dot{m}/\rho_\infty u_\infty A$ determined for each shape is:

Cone	$\dot{m}/\rho_\infty u_\infty A$
10° half-angle	0.002
Blunt 10° half-angle	.02
30° half-angle	.04
Blunt 60° half-angle	.04

The total mass-loss parameter has been specified in previous reports concerning possible effects of ablation on aerodynamics (e.g., refs. 1-7). It is not known, however, whether this parameter is significant for bodies at angle of attack where the mass-loss distribution might be important.

Comparisons of calculated with experimental results for $\alpha = 0^\circ$.- Predicted curves of recession distance, nose radius, and mass loss versus time are compared with the measured results in figures 7 through 9, and, in general, the computed curves agree well with the data. The analytical method used to compute the curves was based on conventional steady-state ablation concepts, with the stagnation heating-rate parameter $\dot{q}_{st}\sqrt{r}$ remaining constant. It was assumed that the model noses ablated spherically and the sides remained conical. As suggested in reference 15, the parameter

$$k = \dot{q}_c(h_{eff})_{st}/\dot{q}_{st}(h_{eff})_c$$

was also assumed constant for a given shape. The cone to stagnation-point heating-rate ratio $\dot{q}_c/\dot{q}_{st}$ was determined from an analysis for laminar heat transfer on blunted cones (ref. 16). Details of the method are given in the appendix.

In view of the various assumptions involved, the computed curves agree reasonably well with the experimental data (see figs. 7-9). It can be seen, however, that the computed curves of mass loss with time are extremely sensitive to small changes in k, especially for small-angle cones. The value of k is zero if there is no mass loss from the sides of the cones, as was the case in the present tests for both the initially sharp and initially blunt 10° cones. For $k = 0$, the computed curves of mass loss with time agreed reasonably well with those measured for the 10° cones. However, with k slightly increased to 0.06, the mass loss was greatly overpredicted. The k value of 0.06 was obtained for the assumption of $(h_{eff})_{st}/(h_{eff})_c = 1$ and with $\dot{q}_c/\dot{q}_{st} = 0.06$ (from ref. 16). For the 30° cones there was considerable ablation from the sides, and the mass loss was predicted with $k \approx \dot{q}_c/\dot{q}_{st} = 0.3$ (from ref. 16). No curves were computed for the 60° half-angle cones because of lack of information on $\dot{q}_c/\dot{q}_{st}$.

The experimental values of final radius r_f were measured from enlarged photographs of the ablated models. These photographs show that the ablated tips were not actually spherical (fig. 4), and thus the measured values of r_f in figures 7 to 9 are only approximate.

Forces and Moments for Ablating and Nonablating Models

30° half-angle cones.- For the initially pointed 30° half-angle cones there was no noticeable effect of ablation on the normal-force and pitching-moment coefficients (fig. 10). The axial-force coefficients, however, decreased about 5 percent with ablation throughout the α range studied. This decrease in C_A is consistent with the trend recently observed by Chrusciel and Chang (ref. 7) for ablating 9° half-angle cones of ammonium chloride and paradichlorobenzene. In tests at $M_\infty \approx 11$ and $Re \approx 1.5 \times 10^5$ they found that, for laminar flow and with mass-loss parameters up to about 6 percent, the axial-force coefficients could be reduced as much as 55 percent. Since they found no effects of ablation on axial-force coefficients obtained from integration of pressure data, the appreciable decreases in C_A were attributed primarily to large decreases in skin friction. Thus, from the limited results to date, it appears that effects of ablation on C_A are primarily changes in skin friction. For slender cones in which the skin-friction contribution to C_A is appreciable, large ablation effects might be expected. However, for "not so slender" cones in which the skin-friction contribution is small, only small effects might be expected (unless, of course, the shape changes greatly). For the 30° half-angle cones tested in the present investigation, the computed skin-friction contribution (fig. 10) was only about 5 percent of the predicted total axial force. On the basis of this small skin-friction contribution, the measured reduction in C_A of about 5 percent with ablation was as large as could be expected if essentially all the skin friction were removed. The elimination of all the skin friction is, of course, unlikely, and further tests of cones with various half-angles and ablation rates appear desirable to clarify the preliminary trends.

As shown in figure 10, the variations of C_N, C_{m_B}, and x_{cp}/d with α were predicted closely by Newtonian theory, but C_A versus α was underestimated. As for the 9° half-angle cones of reference 7, C_A at $\alpha = 0°$ was also slightly underestimated by the addition of values from laminar (Blasius) skin-friction theory (e.g., ref. 17) and inviscid cone theory (e.g., ref. 18). In the present investigation the Reynolds number might be low enough that the difference in C_A between experiment and theory could be attributed to small viscous interaction effects which were not included in the theory.

Blunt 10° half-angle cones.- For the 40-percent blunt, 10° half-angle cones there were no measurable effects of ablation gas flow on any of the coefficients (fig. 11). However, C_A increased slightly with time for times greater than about 10 seconds. Note, for example, in figure 11 that the values of C_A are slightly greater for $t \approx 30$ seconds than for $t \approx 10$ seconds. It is believed that this slight increase resulted from both nose blunting (see fig. 4) and balance heating with run time. At the present it is not clear why C_A did not decrease with ablation as it did for the pointed 30°

half-angle cone. Possibly, the mass-loss parameter ($\dot{m}/\rho_\infty u_\infty A = 0.02$) was too small and the nose blunting too large for a decrease to be detected.

The normal forces and pitching moments predicted by Newtonian theory were too large. The axial-force results, however, were given closely by adding computed laminar skin-friction values (ref. 17) to Newtonian values.

Blunt 60° half-angle cones.- As for the blunt 10° half-angle cones, there were no noticeable effects of ablation gas flow on the forces and moments for the blunt 60° half-angle cones with boattail aftersections (fig. 12). It is likely that mass-loss parameters considerably greater than the present 4 percent would be required to affect appreciably the characteristics for these blunt shapes, at least with Teflon as the ablator. However, with very large mass-loss rates for Teflon, it would be difficult to separate ablation-gas effects from shape-change effects.

The 4-percent ablation rate was sufficient to produce easily observable ablation gas layers and appreciable shape changes within the 30-second testing time (see shape changes in fig. 4(d)). For the ablating models an ablation gas layer was always visible over the front face, as shown in the photograph in figure 13(a). For both the ablating and nonablating models a self-illuminated shock layer also appeared ahead of the models (figs. 13(a) and 13(b)). The thickness of this layer measured from the nose to the dark-to-light demarcation line at the front of the illuminated shock region appeared to be the same whether an ablating or nonablating model was tested. At the present time, however, it is uncertain whether the bow shock was actually located at the demarcation line. Problems of camera alinement, lighting, and flow-field distortion make it difficult to determine precise flow-field measurements from the photographs.

The force and moment characteristics (fig. 12) for this configuration were not predicted satisfactorily by Newtonian theory. Although Newtonian theory closely predicted C_N versus α, the predicted C_A was too large and the center of pressure was more rearward than measured (fig. 12). The too far rearward center-of-pressure prediction was also observed in reference 19 for 45° and 50° half-angle cones at hypersonic Mach numbers. Newtonian theory appears to be adequate only for predicting center-of-pressure positions for sharp cones of about 40° half-angle and less (ref. 19). For the present tests the center of pressure as well as the axial force was probably influenced slightly by attached flow over the aftersection. Photographs from oil-flow studies showed the flow to be attached over most of the aftersection (fig. 14). If the flow had separated over the entire aftersection, the values of C_A probably would have been slightly smaller than those measured.

C_A versus θ for large-angle cones.- In figure 15, theoretical curves of C_A versus cone half-angle θ for large-angle cones at $\alpha = 0°$ are compared with experimental data from the present tests and from reference 19. The comparisons show that for θ up to at least 50° inviscid cone theory can be used to predict accurately the axial-force coefficients. However, for θ greater than about 57°, the bow shock detaches and other theories must be used. At the present time only the Newtonian and modified Newtonian methods

are amenable to easy application. As shown in figure 15, the experimental results for the 60° half-angle conical models are bracketed by the Newtonian ($C_{p_{st}} = 2$) and modified Newtonian ($C_{p_{st}} = 1.83$) predictions.

CONCLUDING REMARKS

Axial-force, normal-force, and pitching-moment coefficients were measured for ablating Teflon and nonablating metallic pointed 30° half-angle cones, blunted 10° half-angle cones, and blunted 60° half-angle cones with boattail aftersections. For moderate mass-loss rates up to about 4 percent and with laminar flow, there were no appreciable effects of ablation on the forces and moments. The axial-force coefficients for the 30° half-angle cones were affected the most, but they decreased only about 5 percent with ablation throughout the studied angle-of-attack range (0° to 20°). Previous tests of slender pointed cones (9° half-angle) at about the same mass-loss rates indicated much larger percentage decreases in axial force; the decreases were attributed primarily to decreases in skin friction. A loss in stability with ablation was also noted for slender cones. It appears that, at least for moderate ablation, the forces and moments for only slender pointed cones are influenced appreciably by ablation-gas flow. However, further tests of cones with half-angles from about 10° to 30° and for various materials and mass-loss rates appear desirable before a detailed evaluation can be made.

The forces and moments for the pointed 30° half-angle cones were adequately predicted with Newtonian theory. However, for the blunted 10° half-angle cones, the normal forces were considerably less than those predicted by Newtonian theory, and for the blunt 60° half-angle conical models, the predicted axial forces were larger and the centers of pressure more rearward (by about 0.15 diam) than were measured. At the present time there is a lack of an adequate theory and of experimental data for both sharp and blunt cones with half-angles greater than about 50°. Because of possible use of large-angle cones for planetary entry vehicles, further study is suggested.

A method for estimating cone recession and mass loss with time has been assessed for the present test conditions. Computed curves agreed reasonably well with experimental measurements from ablation tests of pointed 10° half-angle cones, 40-percent blunt 10° half-angle cones, and pointed 30° half-angle cones. Curves were not computed, however, for the blunt 60° half-angle cones because of lack of theory and experiment for the heating-rate distribution over the faces of large-angle cones.

Ames Research Center
National Aeronautics and Space Administration
Moffett Field, Calif., 94035, March 22, 1967
124-07-02-23-00-21

APPENDIX

CONE RECESSION AND MASS LOSS DUE TO ABLATION

Cone recession was first computed following the assumptions used in reference 15. Then the mass loss was estimated from the computed recession distance. Although for a cone the tip dimensions and heat-transfer rates change constantly, conventional steady-state ablation concepts were used. As ablation occurred, the front of the cone was assumed to remain essentially spherical (sketch (a)).

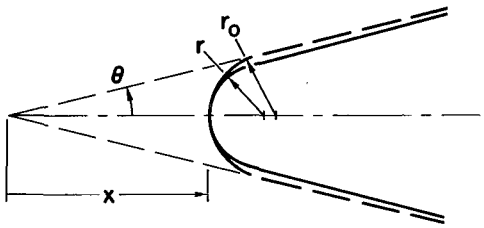

Sketch (a)

The effective heats of ablation are expressed by

$$\left.\begin{aligned} h_{eff} &= \frac{\dot{q}}{\dot{m}} \\ (h_{eff})_{st} &= \frac{\dot{q}_{st}}{\rho_m(dx/dt)} \\ (h_{eff})_c &= \frac{\dot{q}_c}{\rho_m(-dr/dt)} \end{aligned}\right\} \tag{1}$$

Although most of the mass loss is ablated off the front, some is generally ablated off the side (sketch (a)). From equations (1),

$$\frac{r_o - r}{x} \approx \frac{\dot{q}_c}{\dot{q}_{st}} \frac{(h_{eff})_{st}}{(h_{eff})_c} = k \tag{2}$$

The nose radius without mass loss from the side is expressed by

$$r_o = \frac{x \sin \theta}{1 - \sin \theta} \tag{3}$$

Substituting equation (3) into equation (2) gives

$$r \approx \left(\frac{\sin \theta}{1 - \sin \theta} - k\right) x \tag{4}$$

For tests in arc-heated wind tunnels, $\dot{q}_{st}\sqrt{r}$ is usually kept constant during a run, as was the case for the present study. Multiplying both sides of equations (1) by $\sqrt{r}$ and rearranging gives

$$\sqrt{r}\,\frac{dx}{dt} = \frac{\dot{q}_{st}\sqrt{r}}{(h_{eff})_{st}\rho_m} \tag{5}$$

Substituting equation (4) into equation (5) gives

$$\int_{x_i}^{x_f} x^{1/2}\,dx \approx \frac{\dot{q}_{st}\sqrt{r}}{(h_{eff})_{st}\rho_m}\left(\frac{\sin\theta}{1-\sin\theta}-k\right)^{-1/2}\int_{t_i}^{t_f} dt \tag{6}$$

Integrating equation (6) between the indicated limits then gives the final recession distance as

$$x_f \approx \left\{\left[\frac{3}{2}\frac{\dot{q}_{st}\sqrt{r}}{(h_{eff})_{st}\rho_m}\right]\frac{t_f - t_i}{\left(\frac{\sin\theta}{1-\sin\theta}-k\right)^{1/2}} + x_i^{3/2}\right\}^{2/3} \tag{7}$$

The corresponding radius of the ablated tip also was estimated. By differentiating equation (4) and substituting it into equation (5) we obtain

$$\int_{r_i}^{r_f}\sqrt{r}\,dr \approx \frac{\dot{q}_{st}\sqrt{r}}{(h_{eff})_{st}\rho_m}\left(\frac{\sin\theta}{1-\sin\theta}-k\right)\int_{t_i}^{t_f} dt \tag{8}$$

With $\dot{q}_{st}\sqrt{r}$ assumed constant, integrating equation (8) gives

$$r_f \approx \left\{\left[\frac{3}{2}\frac{\dot{q}_{st}\sqrt{r}}{(h_{eff})_{st}\rho_m}\right]\left(\frac{\sin\theta}{1-\sin\theta}-k\right)(t_f - t_i) + r_i^{3/2}\right\}^{2/3} \tag{9}$$

To compute recession distance from equation (7) reasonable estimates of k, $\dot{q}_{st}\sqrt{r}$, and $(h_{eff})_{st}$ had to be made. Values of k (from eq. (2)) are primarily influenced by $\dot{q}_c/\dot{q}_{st}$. As in reference 15, values of $\dot{q}_c/\dot{q}_{st}$ for laminar heat transfer on blunted cones were obtained from plots in reference 16 (also given in ref. 15). Following reference 15, it was further assumed (for estimative purposes) that the ratio of $(h_{eff})_{st}$ to $(h_{eff})_c$ is unity for a subliming material such as Teflon (used in the present study).

The quantity $\dot{q}_{st}\sqrt{r}$ was measured with a hemispherical-nosed calorimeter. A simplified form of Fay and Riddell's heating-rate relationship (ref. 11) (used also in refs. 9 and 12) was used:

$$\dot{q}_{st}\sqrt{r} \approx 0.042\sqrt{p_{st}}\,(h_t - h_{cw}) \tag{10}$$

In this relation h_t was obtained by the "sonic flow" method (e.g., refs. 12-14). Values of $\dot{q}_{st}\sqrt{r}$ from the calorimeter measurements and from equation (10) agreed to within about 10 percent.

For Teflon the effective heat of ablation was calculated from the empirical relation

$$\left.\begin{aligned} h_{eff} &= 38.3(\Delta h_{hw})^{0.49} \\ &\approx 38\sqrt{h_t - h_{cw}} \end{aligned}\right\} \tag{11}$$

for conditions in the present study. This formula was derived in reference 20 from a study of Teflon ablation data from various sources and for total enthalpies up to about 18,000 Btu/lb.

The mass loss due to ablation was computed from

$$\Delta m = \rho_m \Delta V = \rho_m (V_i - V_f) \tag{12}$$

where $\rho_m \approx 134$ lb/ft^3 for Teflon.

The initial volume was taken as the sum of the volumes of a spherical nose segment and a conical frustum, as given by

$$V_i = \frac{\pi}{3} r_b^3 \left[\eta_i^3 (1 - \sin\theta_i)^2 (2 + \sin\theta_i) + \left(\frac{1 - \eta_i \cos\theta_i}{\tan\theta_i}\right)(1 + \eta_i \cos\theta_i + \eta_i^2 \cos^2\theta_i)\right] \tag{13}$$

where $\eta_i = r_i/r_b$.

Two different estimates of the final volume were obtained from the similar expression

$$V_f = \frac{\pi}{3} r_b^3 \left[\eta_f^3 (1 - \sin\theta_f)^2 (2 + \sin\theta_f) + \left(\frac{1 - \eta_f \cos\theta_f}{\tan\theta_f}\right)(1 + \eta_f \cos\theta_f + \eta_f^2 \cos^2\theta_f)\right] \tag{14}$$

For one estimate negligible ablation from the side of the cone was assumed so that $\theta_f = \theta_i$ (sketch (b)) and $\eta_f = r_{o_f}/r_b$ with

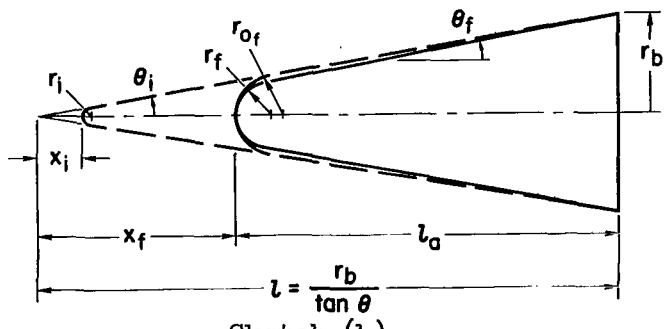

Sketch (b)

$$r_{o_f} = \frac{x_f \sin\theta_i}{1 - \sin\theta_i} \tag{15}$$

For the other estimate it was assumed that ablation from the side of the cone left the configuration conical from the ablated nose radius r_f (by eq. (9)) to the base radius r_b (see sketch (b)).

The base radius was assumed to be unaffected by ablation so that $\eta_f = r_f/r_b$, and the final cone angle was computed from

$$\sin \theta_f = \frac{-2r_f(l_a - r_f) + \sqrt{4r_f^2(l_a - r_f)^2 - 4[(l_a - r_f)^2 + r_b^2](r_f^2 - r_b^2)}}{2[(l_a - r_f)^2 + r_b^2]} \tag{16}$$

where $l_a = (r_b/\tan \theta_i) - x_f$.

REFERENCES

1. Syvertson, Clarence A.; and McDevitt, John B.: Effects of Mass Addition on the Stability of Slender Cones at Hypersonic Speeds. AIAA J., vol. 1, no. 4, April 1963, pp. 939-940.

2. Syvertson, C. A.; and McDevitt, J. B.: Effects of Mass-Transfer Cooling on the Static Stability and Dynamic Motions of Slender Entry Vehicles. Trans. Eighth Symp. on Ballistic Missile and Space Technology, vol. III, San Diego, Calif., Oct. 15-18, 1963.

3. Sacks, I.; and Schurmann, E. E.: Aerodynamic Phenomena Associated With Advanced Reentry Systems. AVCO RAD-TM-63-79, Dec. 1963.

4. Seiff, Alvin: Developments in Entry Vehicle Technology. AIAA Paper 64-528, 1964.

5. Grimes, James H., Jr.; and Casey, John J.: Influence of Ablation on the Dynamics of Slender Re-Entry Configurations. J. Spacecraft Rockets, vol. 2, no. 1, Jan.-Feb. 1965, pp. 106-108.

6. Ericsson, Lars Eric; and Reding, J. Peter: Ablation Effects on Vehicle Dynamics. AIAA Paper 66-51, 1966.

7. Chrusciel, G. T.; and Chang, S. S.: Effects of Ablation on Hypersonic Aerodynamic Stability Characteristics. AIAA Paper 66-410, 1966.

8. Eschenbach, R. C.; and Skinner, G. M.: Development of Stable, High Power, High Pressure Arc Air Heaters for a Hypersonic Wind Tunnel. WADD TR 61-100, July 1961.

9. Jorgensen, Leland H.; and Graham, Lawrence A.: Predicted and Measured Aerodynamic Characteristics for Two Types of Atmosphere-Entry Vehicles. NASA TM X-1103, 1965.

10. Reinhardt, Walter A.; and Baldwin, Barrett S., Jr.: A Model for Chemically Reacting Nitrogen-Oxygen Mixtures With Application to Nonequilibrium Air Flow. NASA TN D-2971, 1965.

11. Fay, J. A.; and Riddell, F. R.: Theory of Stagnation Point Heat Transfer in Dissociated Air. J. Aerospace Sci., vol. 25, no. 2, Feb. 1958, pp. 73-85, 121.

12. Winovich, Warren: On the Equilibrium Sonic-Flow Method for Evaluating Electric-Arc Air-Heater Performance. NASA TN D-2132, 1964.

13. Jorgensen, Leland H.; and Baum, Gayle M.: Charts for Equilibrium Flow Properties of Air in Hypervelocity Nozzles. NASA TN D-1333, 1962.

14. Jorgensen, Leland H.: The Total Enthalpy of a One-Dimensional Nozzle Flow With Various Gases. NASA TN D-2233, 1964.

15. Stetson, Kenneth F.: Preliminary Cone-Ablation Results. J. Spacecraft Rockets, vol. 2, no. 2, March-April 1965, pp. 232-238.

16. Lees, Lester: Laminar Heat Transfer Over Blunt-Nosed Bodies at Hypersonic Flight Speeds. Jet Propulsion, vol. 26, no. 4, April 1956, pp. 259-269, 274.

17. Truitt, Robert W.: Fundamentals of Aerodynamic Heating. The Ronald Press, N. Y., 1960, pp. 34-57.

18. Ames Research Staff: Equations, Tables, and Charts for Compressible Flow. NACA Rep. 1135, 1953.

19. Penland, Jim A.: A Study of the Stability and Location of the Center of Pressure on Sharp, Right Circular Cones at Hypersonic Speeds. NASA TN D-2283, 1964.

20. Hiester, Nevin K.; and Clark, Carroll F.: Feasibility of Standard Evaluation Procedures for Ablating Materials. NASA CR-379, 1966.

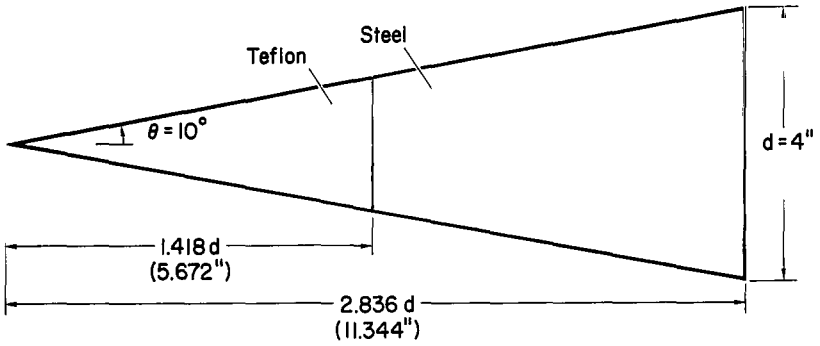

(a) 10° half-angle cone.

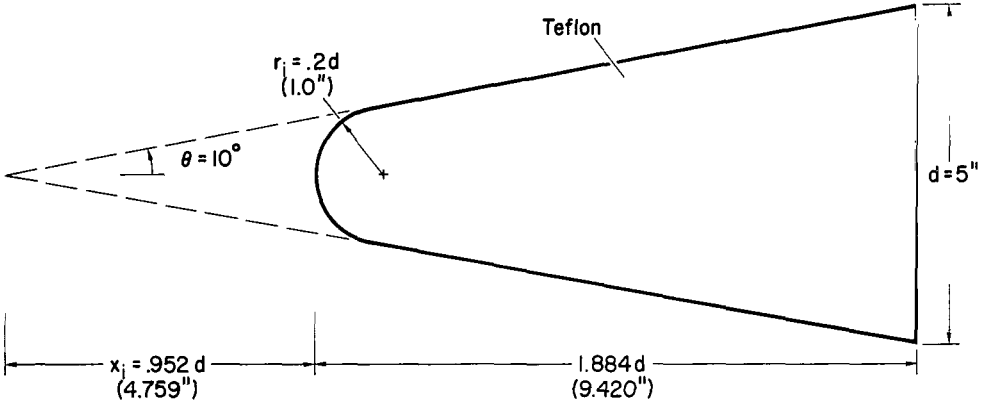

(b) Blunt, 10° half-angle cone.

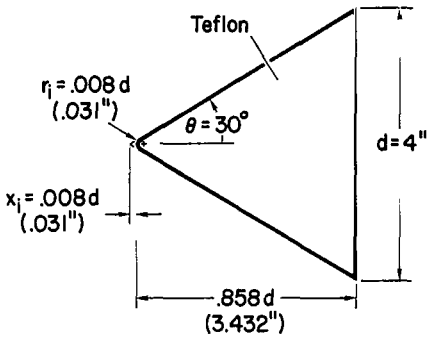

(c) 30° half-angle cone.

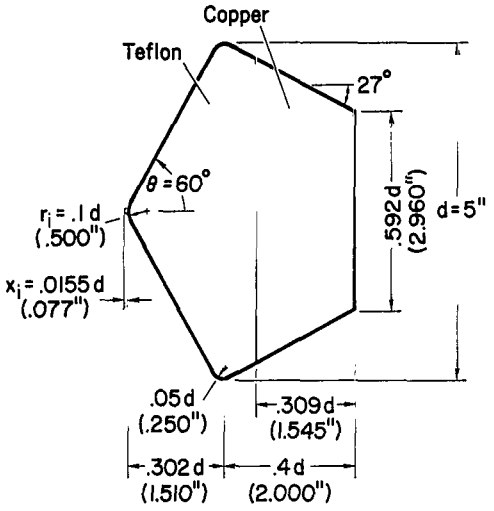

(d) Blunt, 60° half-angle cone.

Figure 1.- Models for ablation tests.

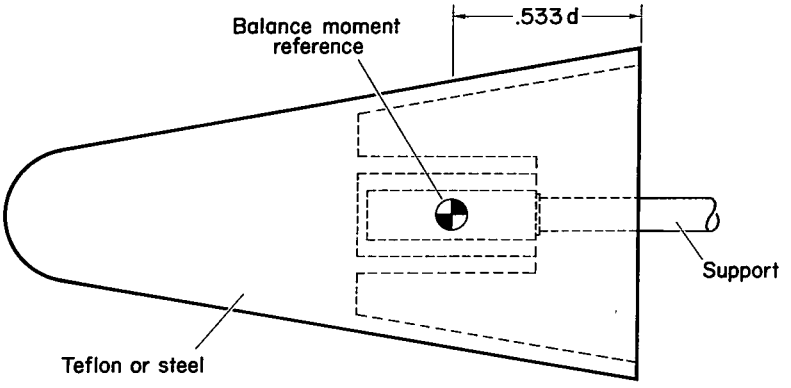

(a) Blunt, 10° half-angle cone.

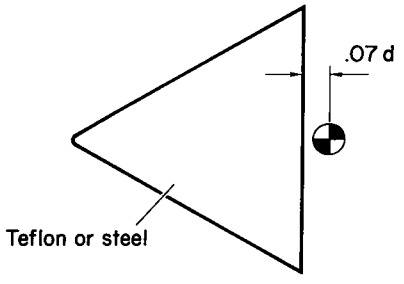

(b) 30° half-angle cone.

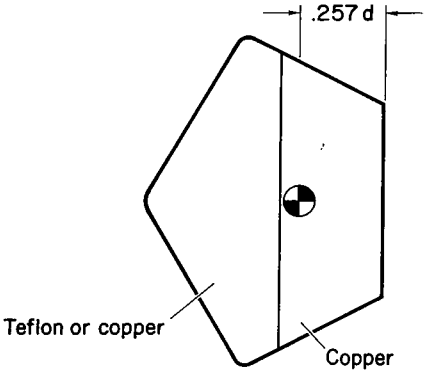

(c) Blunt, 60° half-angle cone.

Figure 2.- Models for force and moment tests.

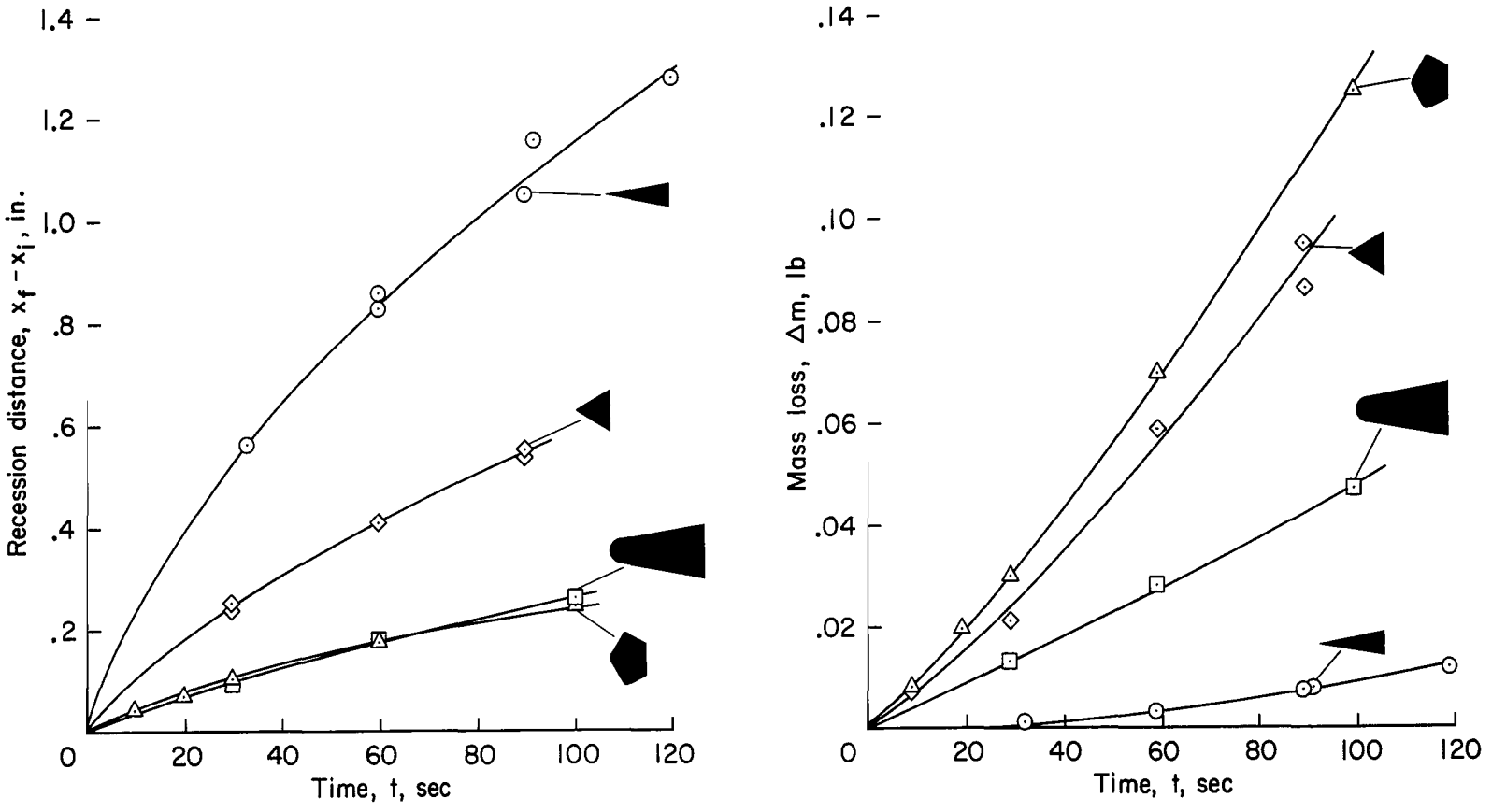

Figure 3.- Experimental recession distance and mass loss versus time for ablating Teflon models at $\alpha = 0^{\circ}$.

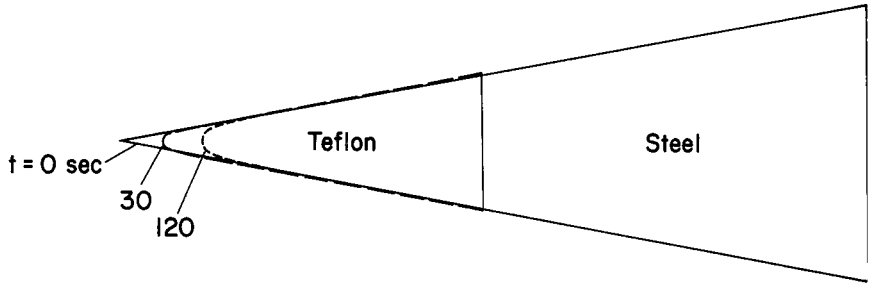

(a) 10° half-angle cone.

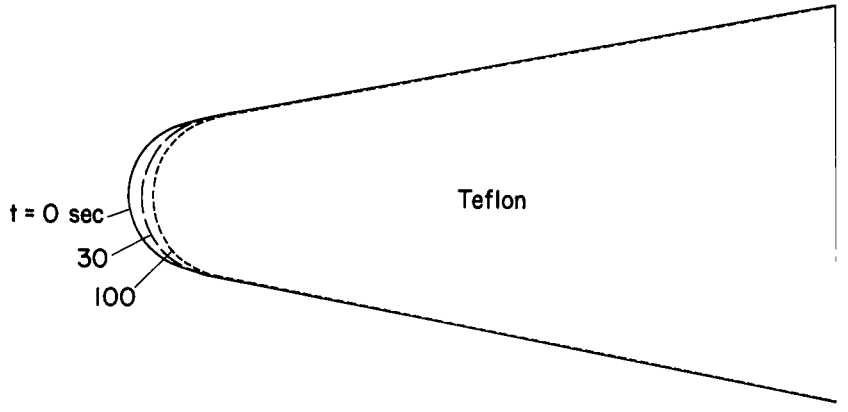

(b) Blunt, 10° half-angle cone.

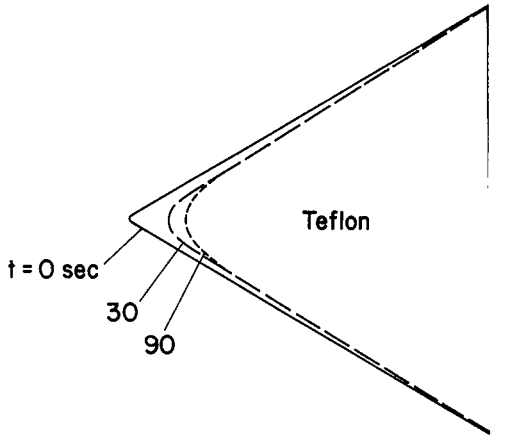

(c) 30° half-angle cone.

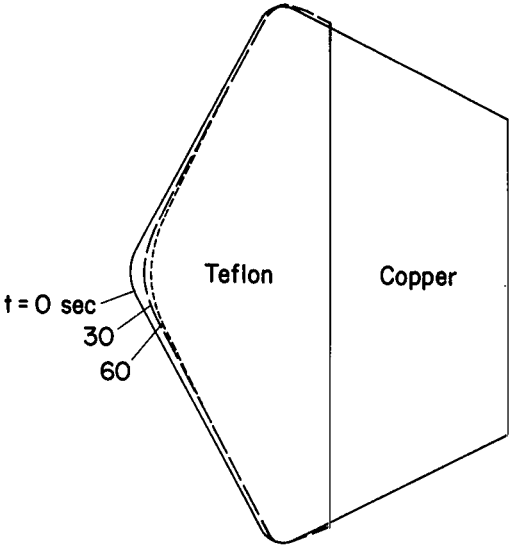

(d) Blunt, 60° half-angle cone.

Figure 4.- Model contours after ablation tests at $\alpha = 0^{\circ}$.

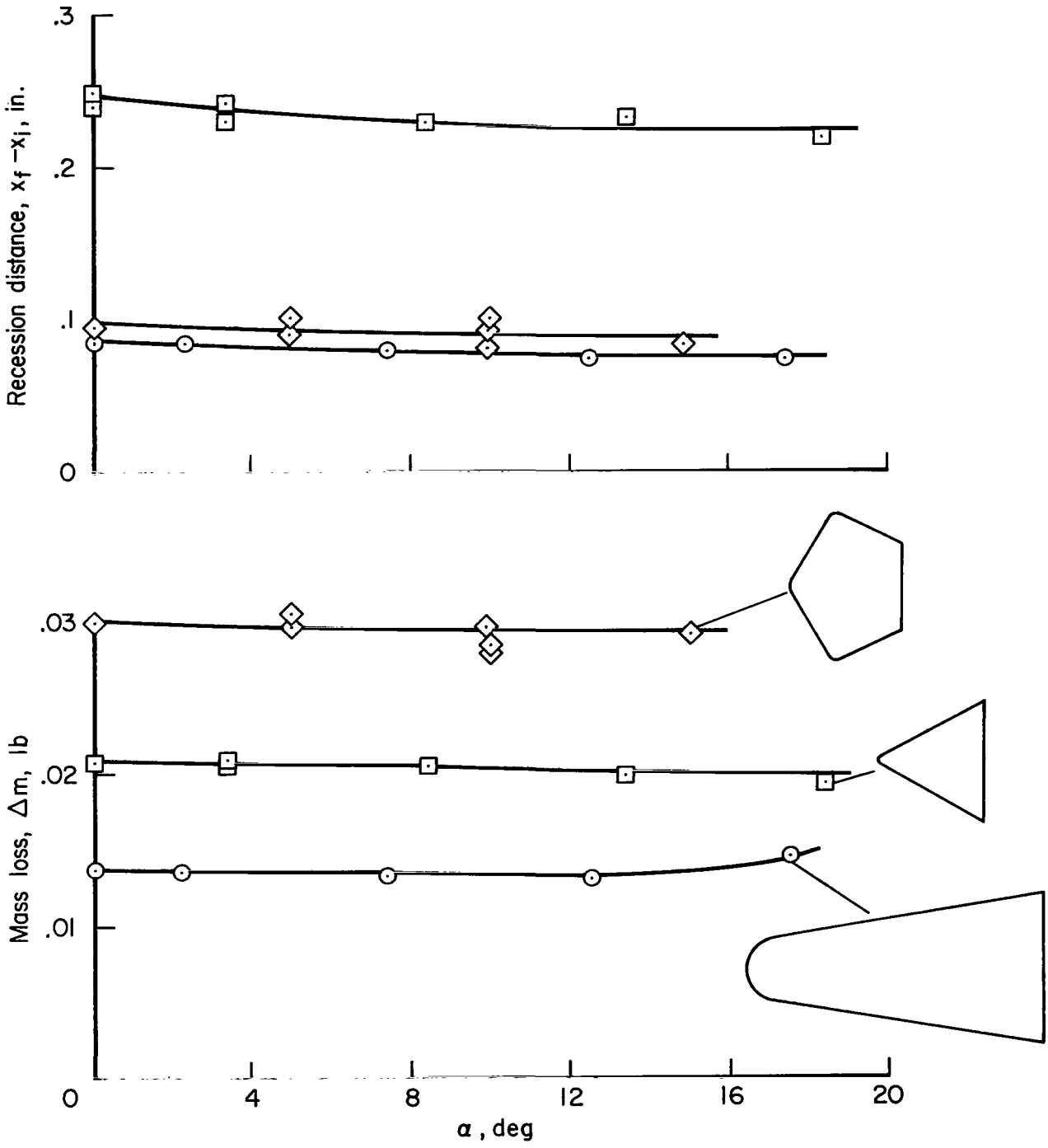

Figure 5.- Effect of angle of attack on recession distance and mass loss for Teflon models exposed 30 seconds in test stream.

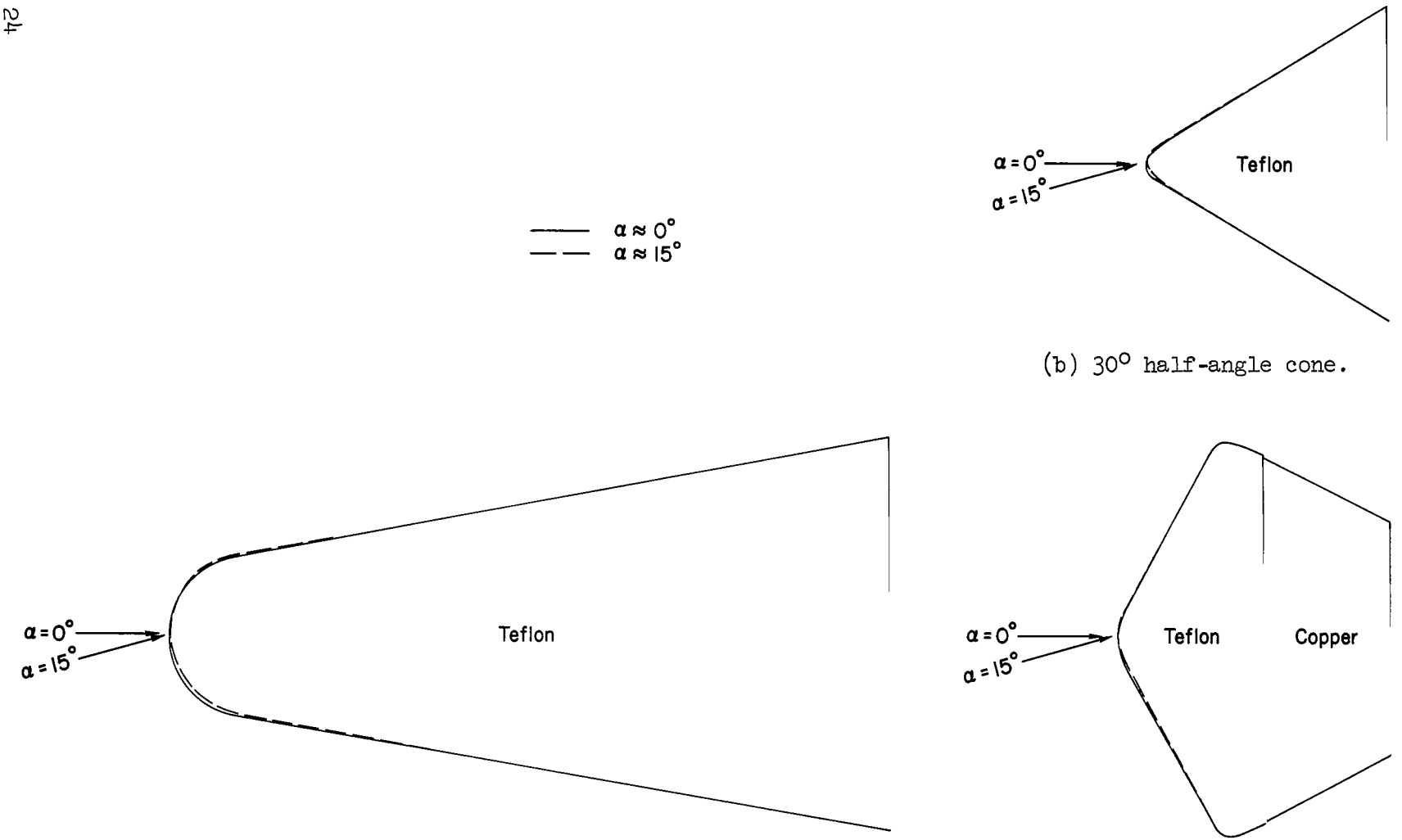

(b) 30° half-angle cone.

(a) Blunt, 10° half-angle cone.

(c) Blunt, 60° half-angle cone.

Figure 6.- Effect of angle of attack on contours of Teflon models exposed 30 seconds in test stream.

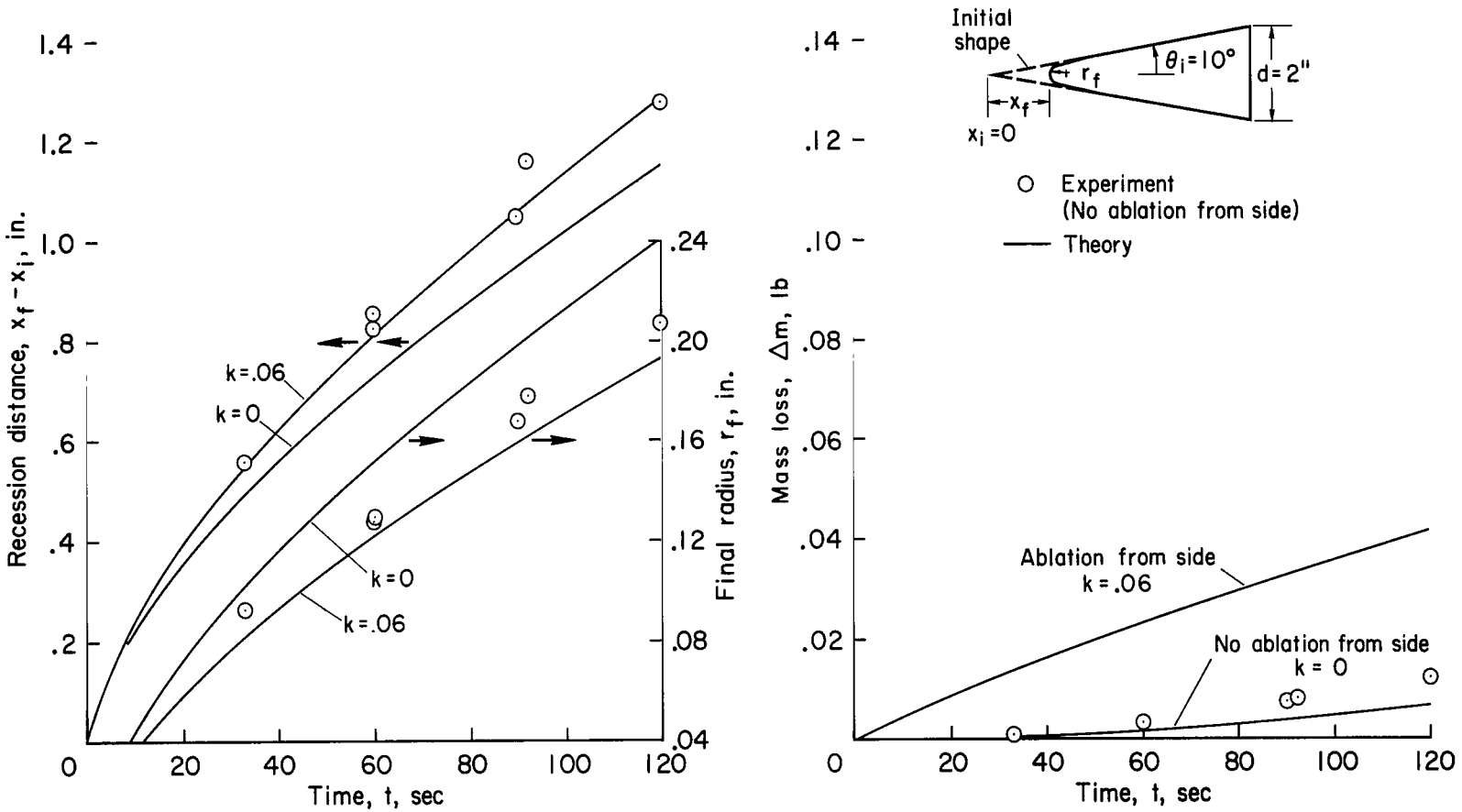

Figure 7.- Comparisons of calculated with experimental ablation results for 10° half-angle conical models of Teflon; $\alpha = 0°$.

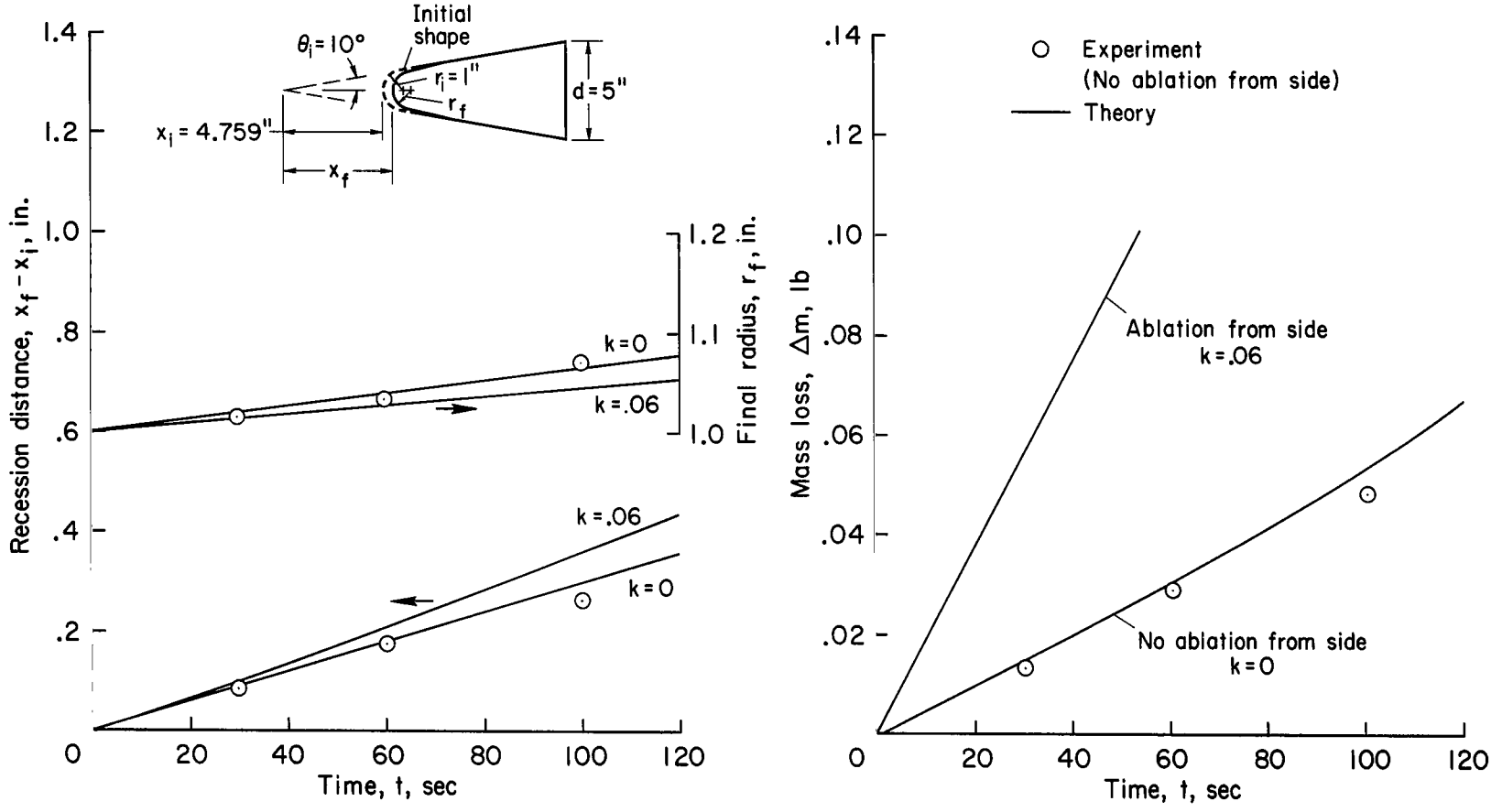

Figure 8.- Comparisons of calculated with experimental ablation results for 40° blunt, 10° half-angle conical models of Teflon; $\alpha = 0°$.

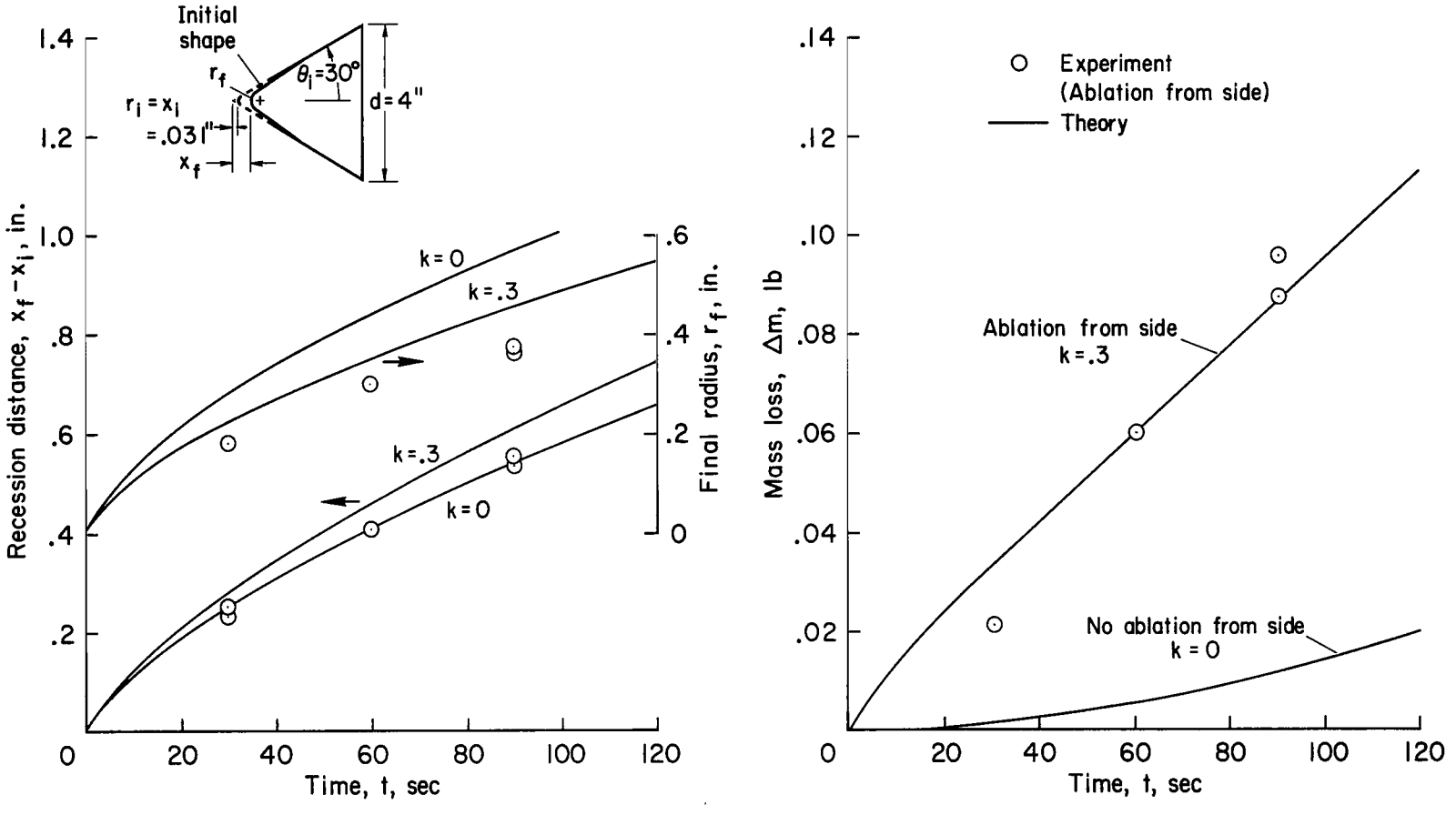

Figure 9.- Comparisons of calculated with experimental ablation results for 30° half-angle conical models of Teflon; $\alpha = 0°$.

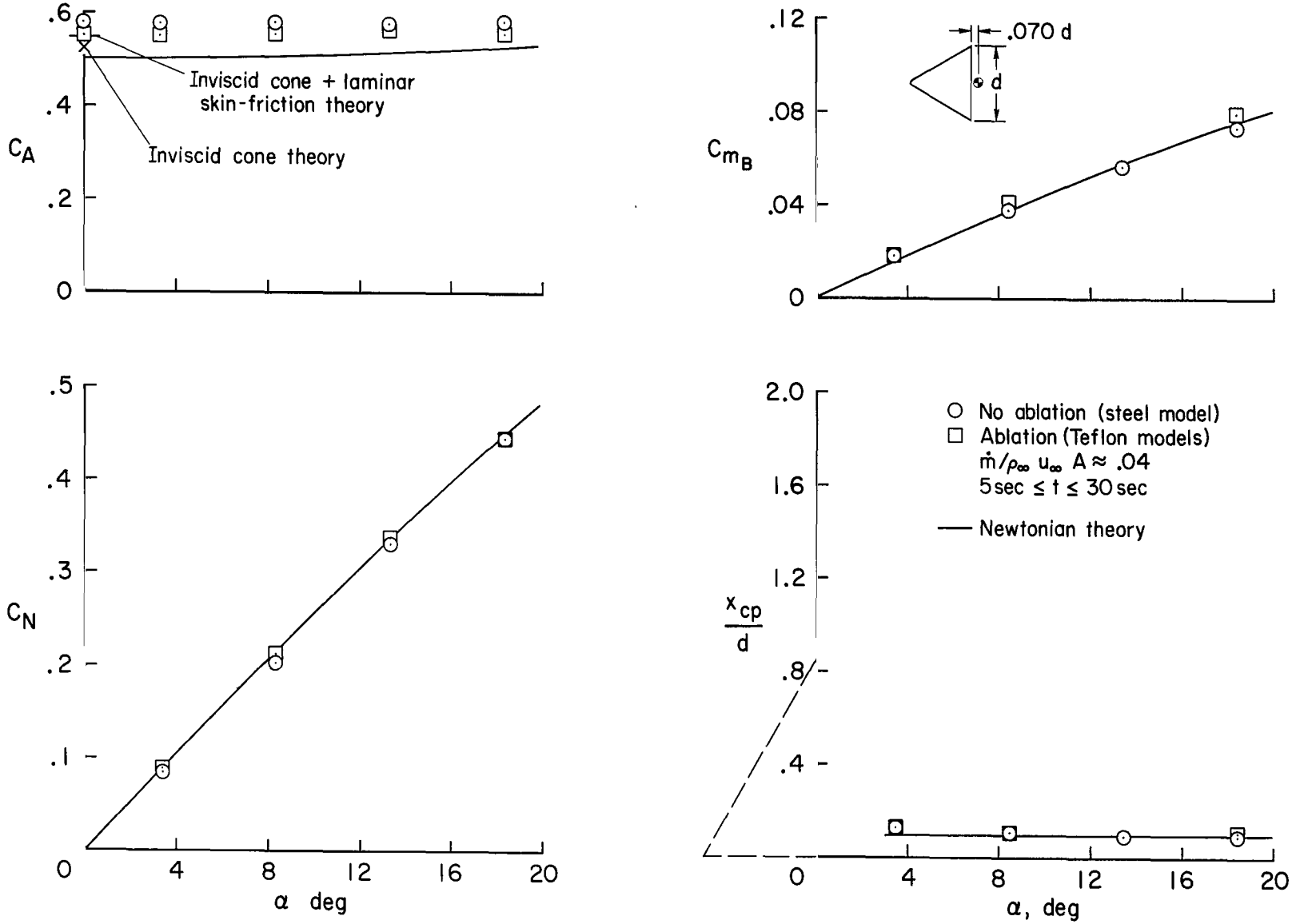

Figure 10.- Aerodynamic characteristics of 30° half-angle conical models with and without ablation.

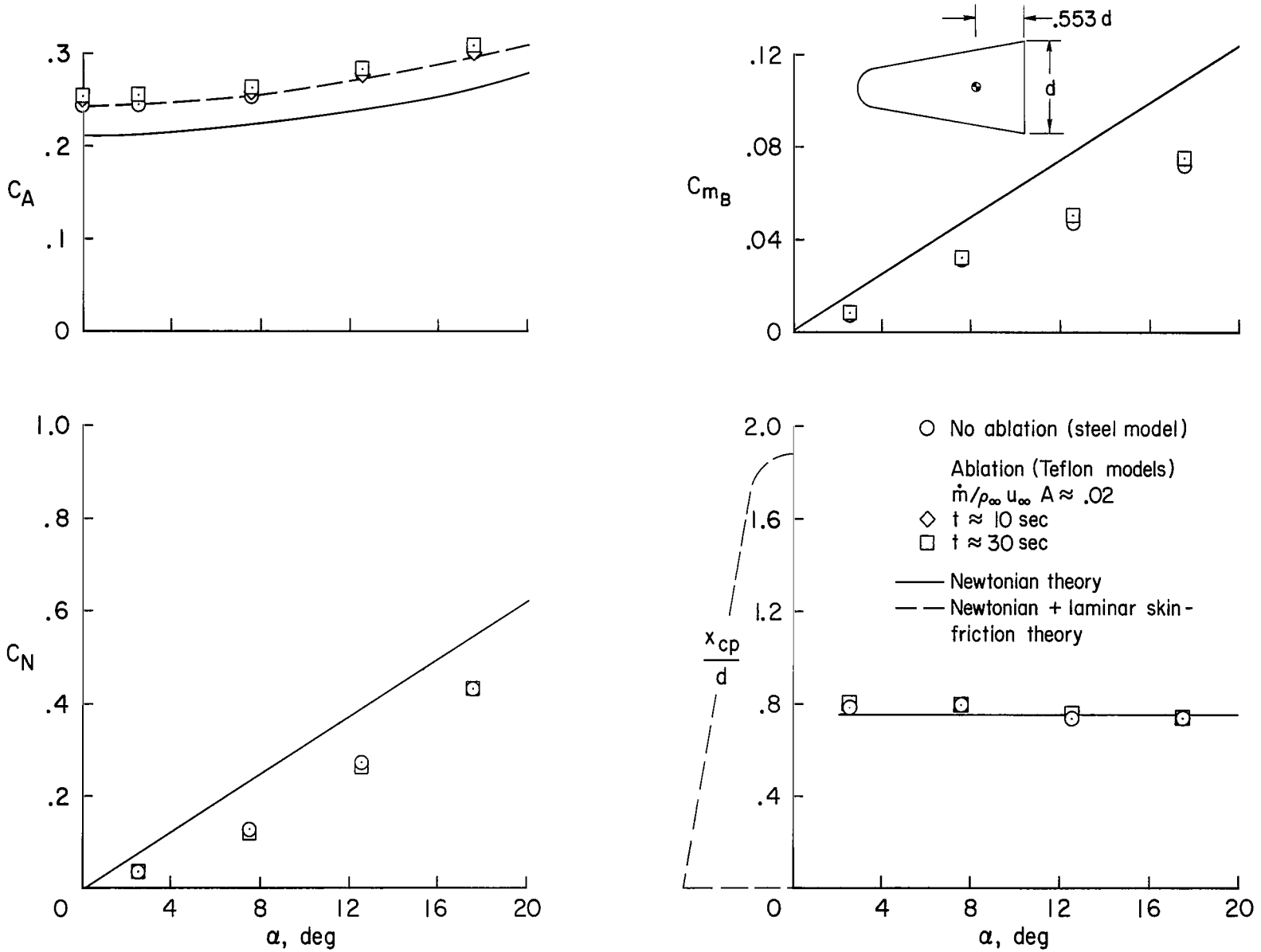

Figure 11.- Aerodynamic characteristics of blunt, 10° half-angle conical models with and without ablation.

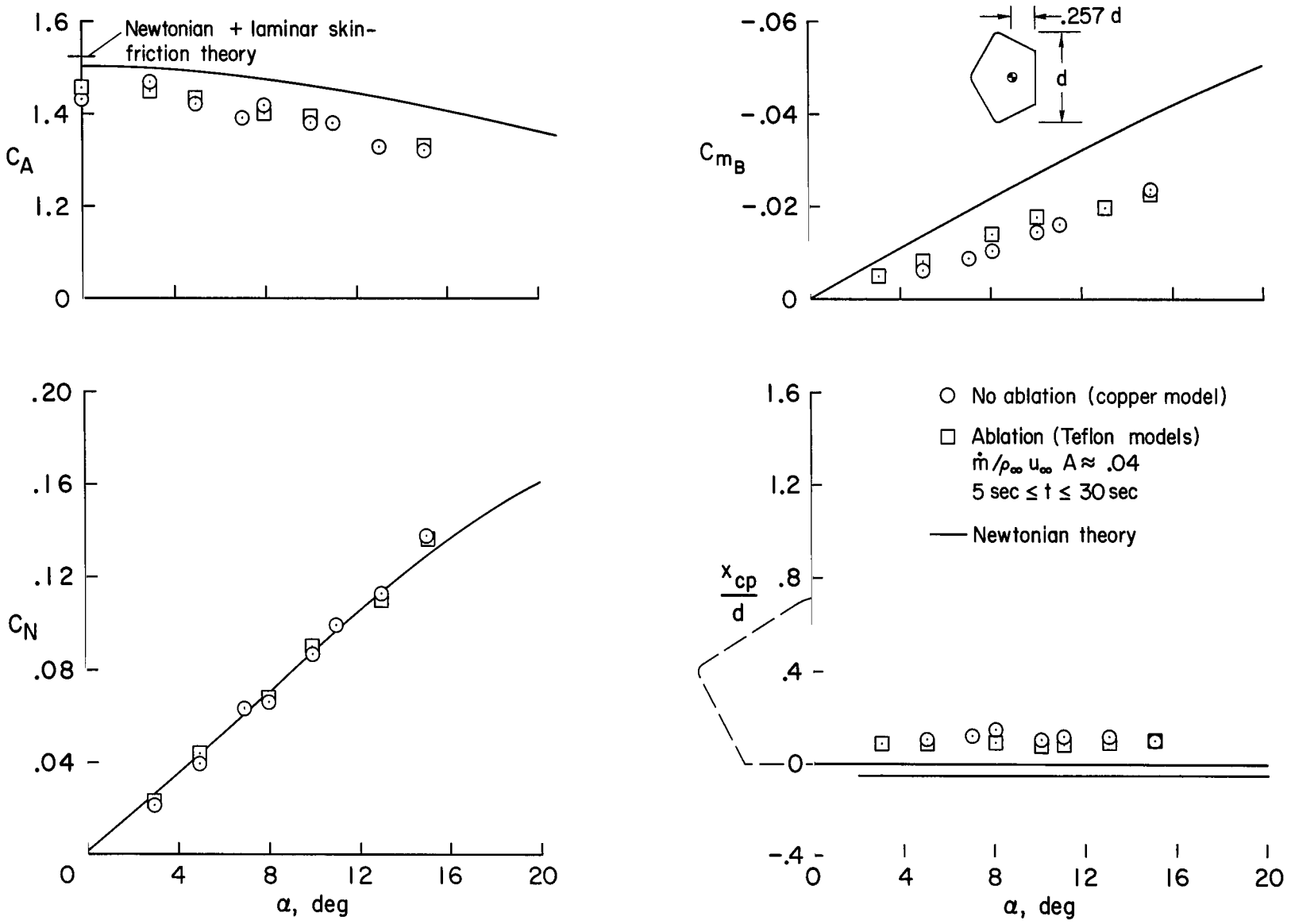

Figure 12.- Aerodynamic characteristics of blunt, 60° half-angle conical models with and without ablation.

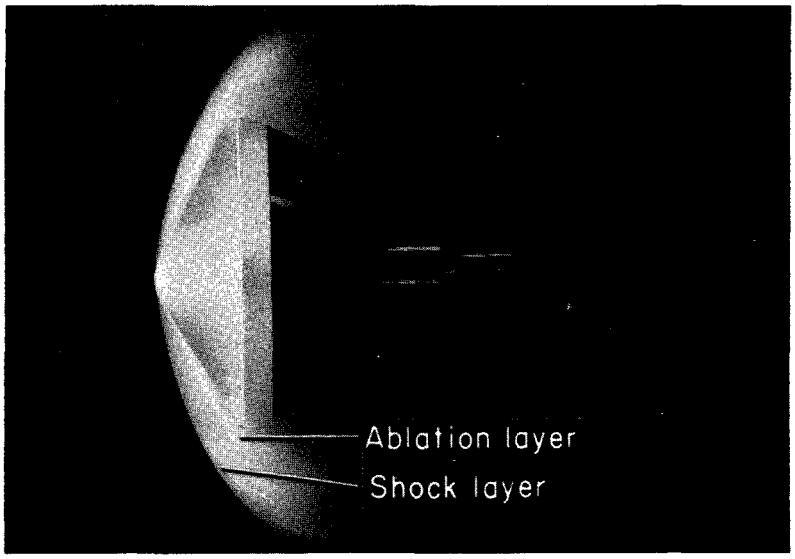

(a) Ablating Teflon nose.

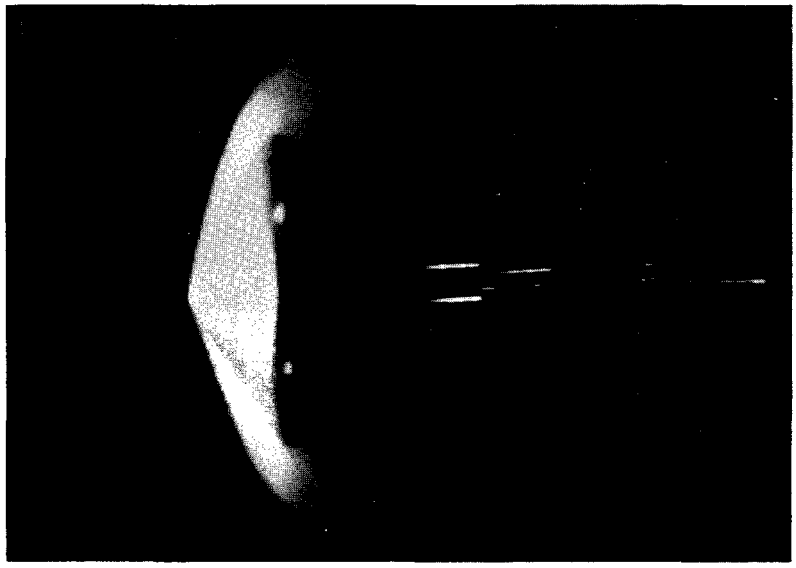

(b) Nonablating copper nose.

Figure 13.- Movie frames from tests of 60° conical models with ablating (Teflon) and nonablating (copper) nose sections; $\alpha \approx 5°$.

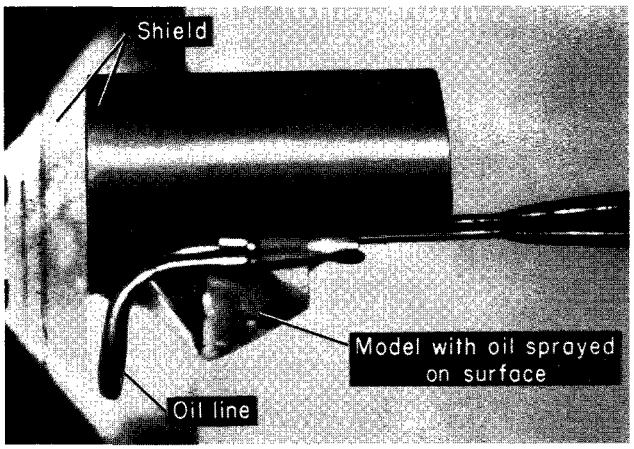

(a) Model with oil-applying shield in place.

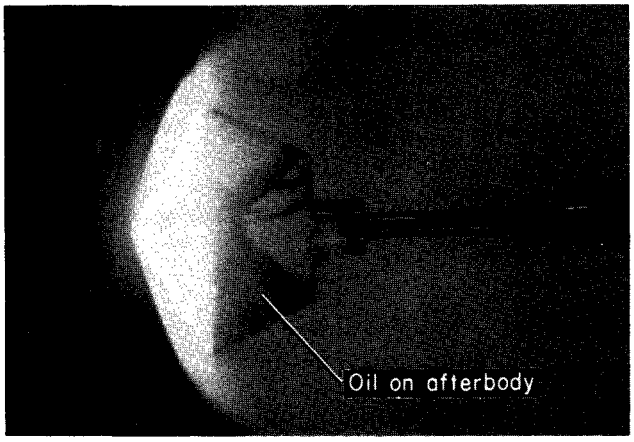

(b) Model immediately after removal of shield.

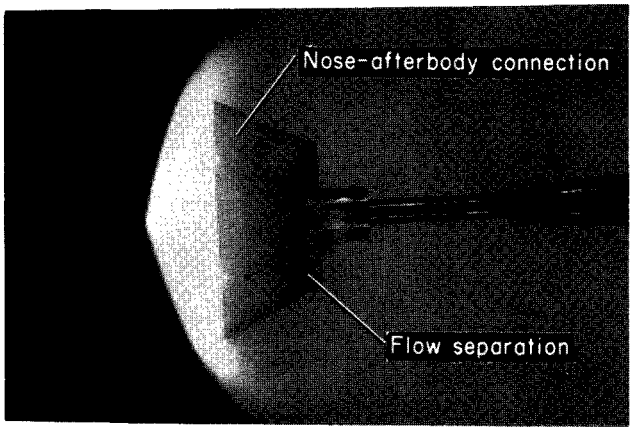

(c) Model several seconds after removal of shield.

Figure 14.- Movie frames from test of 60° conical model (copper painted white) showing oil flow over afterbody; $\alpha \approx 5^{\circ}$.

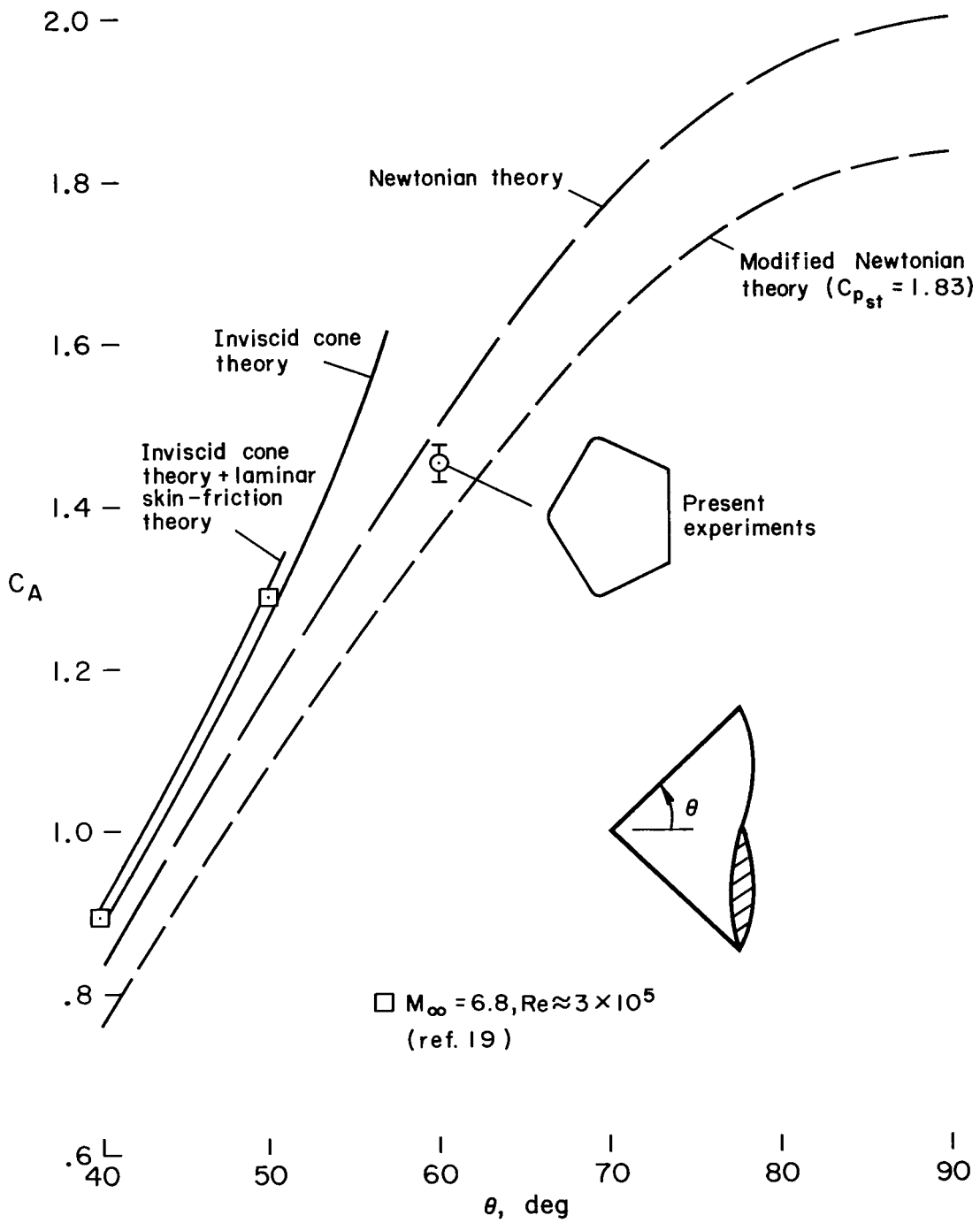

Figure 15.- Axial-force coefficients for large-angle cones at zero angle of attack.

"The aeronautical and space activities of the United States shall be conducted so as to contribute . . . to the expansion of human knowledge of phenomena in the atmosphere and space. The Administration shall provide for the widest practicable and appropriate dissemination of information concerning its activities and the results thereof."

—NATIONAL AERONAUTICS AND SPACE ACT OF 1958

NASA SCIENTIFIC AND TECHNICAL PUBLICATIONS

TECHNICAL REPORTS: Scientific and technical information considered important, complete, and a lasting contribution to existing knowledge.

TECHNICAL NOTES: Information less broad in scope but nevertheless of importance as a contribution to existing knowledge.

TECHNICAL MEMORANDUMS: Information receiving limited distribution because of preliminary data, security classification, or other reasons.

CONTRACTOR REPORTS: Scientific and technical information generated under a NASA contract or grant and considered an important contribution to existing knowledge.

TECHNICAL TRANSLATIONS: Information published in a foreign language considered to merit NASA distribution in English.

SPECIAL PUBLICATIONS: Information derived from or of value to NASA activities. Publications include conference proceedings, monographs, data compilations, handbooks, sourcebooks, and special bibliographies.

TECHNOLOGY UTILIZATION PUBLICATIONS: Information on technology used by NASA that may be of particular interest in commercial and other non-aerospace applications. Publications include Tech Briefs, Technology Utilization Reports and Notes, and Technology Surveys.

Details on the availability of these publications may be obtained from:

SCIENTIFIC AND TECHNICAL INFORMATION DIVISION

NATIONAL AERONAUTICS AND SPACE ADMINISTRATION

Washington, D.C. 20546